https://doi.org/10.7494/miag.2022.2.550.17

SZYMON RĘCZKOWICZ

Mechatronic design of a two-wheeled mobile platform

The article presents the results of work on a project for a two-wheeled self-balancing mobile platform prepared as part of engineering work. The purpose of creating the structure was to enable the increased mobility of an adult over short distances in an urbanized environment.

The whole design work was divided into several parts. In the first stage, requirements were assumed for the design of the device, electrical elements chosen, and a diagram of their electrical connections is presented. In the second part, the created CAD model of the structure is presented and some of mechanical elements described. In order to check the strength of the structure, the FEM analysis of the device body was carried out. The penultimate part was to analyze the problem of the inverted pendulum, which allowed to separate the state space model into a base subsystem and a control stick subsystem necessary to develop the control for the platform. In the last part, a stabilizing algorithm based on the LQR regulator was prepared and the use of sensory fusion in the form of a Kalman filter was focused on in order to increase the accuracy of determining the angle of deflection of the structure.

Finally, simulations were prepared in the Simulink environment in order to check the correctness of the prepared algorithm. The whole was crowned with a summary of the work and setting directions for further research.

Key words: *self-balancing vehicles, Kalman filter, two-wheeled structures*

1. INTRODUCTION

Nowadays, issues related to micromobility, i.e. short-distance travel with the help of small, light and emission-free means of communication, play an increasingly important role [1]. This is due to the fact that currently people mainly care about getting to their destination quickly, and due to the common occurrence of traffic jams, the use of cars is unprofitable over short distances.

The most popular and oldest devices related to the issue of micromobility are bicycles, however, due to the fact that, like scooters or rollerblades, they require physical effort from the driver in order to set the vehicle in motion, they do not satisfy the need for effortless movement present in part of society. The group of vehicles that allows to meet all these conditions are "personal transport devices" (so-called PT), which are defined as "an electrically powered vehicle, excluding an electric scooter, without a seat and pedals, structurally designed to move only with the driver on this vehicle". Self-balancing vehicles have gained great popularity in this group [2].

Self-balancing vehicles are single-axle devices equipped with motorized wheels (or wheel) connected to a movable base on which the driver stands. The self-balancing function, which most distinguishes these vehicles from others designed for independent driving, is the result of a complex algorithm uploaded to the control unit, which allows you to react to changes in the vehicle's yaw detected by sensors located in the vehicle.

A person can "disrupt" this system by leaning, causing the system to perform a procedure to re-stabilize the device, resulting in vehicle movement.

To sum up, it was decided to work on the structure due to the observable demand for electrically powered vehicles designed to move over short distances in urban areas.

2. DESIGN ASSUMPTIONS

At the beginning, the author conducted the state of the art and the research into the applicable norms and laws [2], as well as research into the average weight [3] and posture of a person [4]. As a result of this analysis, the following requirements were established:

- The structure is to be a single platform with a mounted steering rod where the tilt of the structure and the deviation of the rod are detected.
- The maximum speed at which the vehicle can move on a flat surface is v_{max} = 20 km/h (in accordance with the maximum permitted speed for PT vehicles) [2].
- Permissible weight of the transported person m_{max} = 100 kg – determined as the sum of the weight of an average adult male equal to 90 kg (according to research carried in the USA [3]) and clothes carried together with hand luggage as 10 kg.
- Maximum speed when driving with a maximum load under 5° surface inclination – v_{inc} = 10 km/h.

During the selection of elements for this project, the above-mentioned assumptions were followed.

3. ELECTRICAL PART

3.1. Engine

The process of selecting elements for the project began with the selection of engines due to the fact that they are responsible for setting the entire structure in motion. Their poor selection could result in failure to meet the previously presented requirements or prevent the correct implementation of the stabilizing algorithm due to overly slow or inaccurate position change.

In order to initially determine the minimum parameters to be met by the engine, the example of a body on a level was used (Fig. 1).

Using the knowledge of patterns for the body being on an incline, the following were determined:

$$F_g = m \cdot g \tag{1}$$

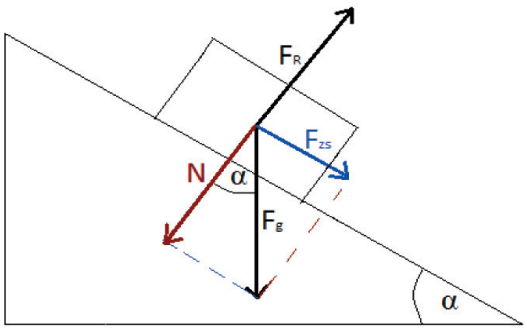

Fig. 1. Body on a slippery slope

The approximate weight is the maximum weight of the transported individual:

$$F_{g\,max} = m_{max} \cdot g = 100 \cdot 9.81 = 981 \text{ N} \tag{2}$$

The angle of inclination of an incline a was taken as 5° to ensure that the condition for the vehicle to move at a speed of 10 km/h at that angle of inclination of the surface would be met.

$$F_z = F_{g\,max} \cdot \sin(\alpha) = 981 \cdot 0.087 = 85.49 \text{ N} \tag{3}$$

Bearing in mind the fact that in the design, each wheel has a separate drive (in order to enable turning), the necessary torque should be divided into two engines:

$$M_{max} = \frac{F_z \cdot r_k}{2} = \frac{85.49 \cdot 0.2}{2} = 8.55 \text{ Nm} \tag{4}$$

In order to determine the necessary power, the linear velocity should be converted into angular:

$$\omega_{inc} = \frac{v_{inc}}{r_k} = \frac{2.78}{0.2} = 13.88 \frac{\text{rad}}{\text{s}} \tag{5}$$

As a result, assuming no slippage, the necessary power was obtained:

$$P_{inc} = M_{max} \cdot \omega_{inc} = 118.74 \text{ W} \tag{6}$$

Considering the above, it was decided to use a pair of NPC-T74 (Fig. 2) engines with the following parameters [5]:

- supply voltage 24 V,
- rotational speed after the gearbox 240 RPM,
- gear design 20 : 1,
- engine ace 6.53 kg,
- maximal output power 1200 W.

Particularly noteworthy is the presence of a built-in gearbox, which allowed the omission of additional elements in order to achieve the necessary torque.

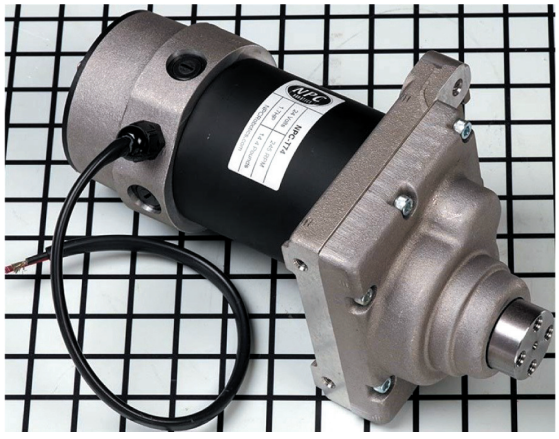

Fig. 2. Engine NPC-T74 [5]

3.2. Controllers

In order to properly control the speed and direction of rotation of the above-mentioned engines, it was necessary to choose the right controller. For the needs of the design, the Sabertooth Dual 60A Speed Controller was chosen, the greatest advantage of which is the simultaneous operation of two drive units using one module.

Nevertheless, a central unit is still required, the main task of which is to read and process signals from sensors, and then use them and a stabilization program uploaded to the unit to determine the control signals that are sent to the motor controller. In the implementation of similar tasks, devices from the Arduino or Raspberry family are most often used. Due to personal experience, it was decided to use Arduino Uno Rev 3.

3.3. Other electrical components

For projects in the field of self-balancing vehicles, it is necessary to detect the angle of inclination and the base, and the speed of its change.

This information is very important in these systems because it is used as input for the stabilizing algorithm. The most popular method of obtaining them accurately is to use the fusion of data from an accelerometer and a gyroscope.

With this in mind, it was decided to select the MPU-6050 unit, in which both of these components are integrated in the form of a single MEMS module.

To read the tilt of the steering set by the driver using the joystick, a mechanical system (described later in the article) was used, which contained an incremental encoder.

An important topic when selecting electrical components for mobile devices is the selection of the correct power supply unit. This is due to the fact that the operating time of the device depends on the capacity of its batteries. The dimensions of energy sources should also be taken into account, because usually in mobile vehicles, due to the limited space, the dimensions of the components play an important role. The last important aspect is the voltage value, which through improper selection may negatively affect the performance of the device or lead to damage to the element.

In self-balancing constructions, the practice is to use two batteries connected in series (usually 12 V) [6]. Despite the increased space, the weight is distributed evenly, which allows you to increase the controllability of the device.

Considering the above, the decision was made to choose a pair of Vision batteries. That specific battery was chosen because it is one of the smallest (151 mm × 98 mm × 95 mm) available 12 V lead batteries that the author managed to find at the time of selecting the elements.

3.4. Electrical diagram

The elements presented in this section alone would not be able to ensure the proper operation of the device. For this purpose, these elements were combined into one system, the connection diagram of which is presented in Figure 3.

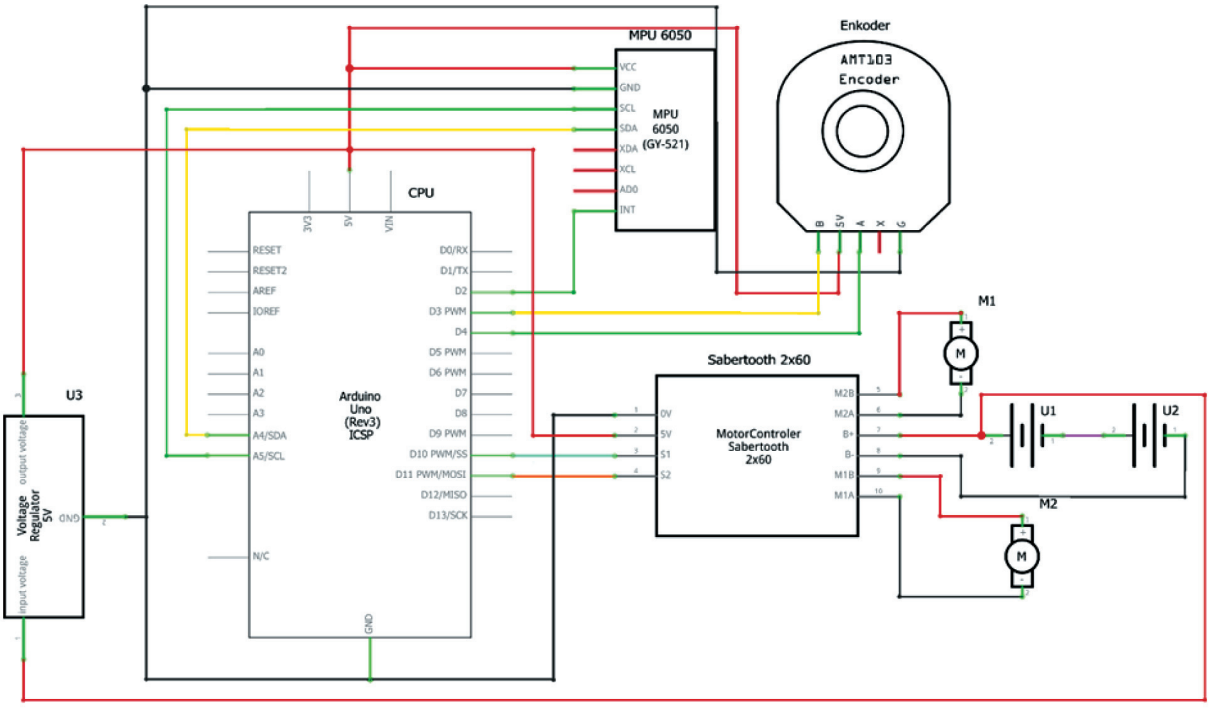

Fig. 3. Electrical diagram of the platform

4. MECHANICAL PART

4.1. Overall dimensions

The process of designing the device model began by determining the overall dimensions that the final construction could not exceed (Fig. 4).

The first parameter that is the width of the device, that is, the distance between the outer edges of the wheels. Taking into account the width of the pavement in accordance with the regulation of the Minister of Transport [4] of up to 2 m, the possibility of two drivers to pass one another while maintaining a safe distance of 0.2 m, plus knowledge of the dimensions of similar devices, the final width of the platform was set at 730 mm.

The length of the device took two factors into account:

1) the average adult's foot length of 250 mm (with research done at the Jan Kochanowski University in Kielce [7]),
2) enabling the storage of all necessary elements inside the structure with their even distribution (facilitation of the stabilization algorithm).

Taking into consideration these factors, the length was determined as 480 mm.

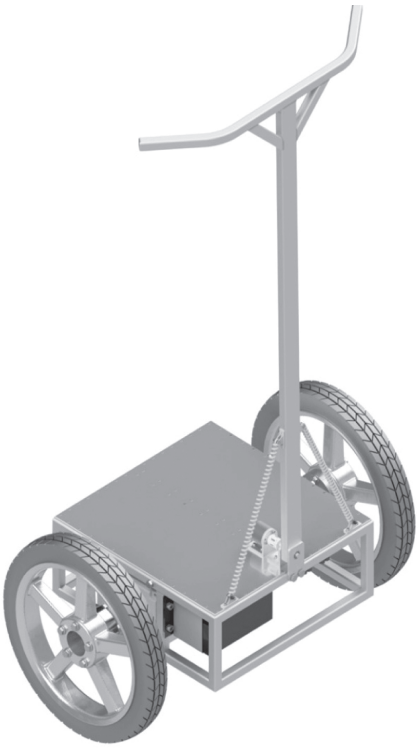

Fig. 4. CAD model of the device

The last dimensional parameter that had to be determined was the height of the structure. In order to determine this, three dimensions had to be added together:

1) The distance of the lower part of the frame from the ground. It was assumed that 100 mm above ground level is a sufficient distance to prevent unwanted interaction with the environment, as a result of which damage could occur to the vehicle.
2) The height of the platform frame. As it must accommodate all electronic parts, its height, especially the height of the engine, which is the basic element of the project, must be taken into account at 200 mm.
3) The distance between the top base housing and the tip of the steer. On the basis of own research, it was determined that the control stick should be approximately 1100 mm long in order to ensure free control of the vehicle.

Summing up all three dimensions, it was assumed that the overall height of the platform should be 1400 mm.

4.2. Elements of the platform base

The whole structure is connected by a frame that allows the manufacturer to mount all the necessary elements in a compact housing while maintaining a passenger weighing up to 100 kg (Fig. 5).

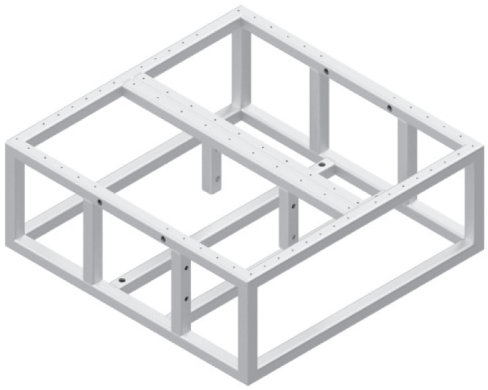

Fig. 5. Designed platform frame

This element was created as a combination of cut closed aluminum profiles with a square cross-section of 20 mm with walls with a thickness of 1.5 mm. The estimated weight of the frame is equal to 2.5 kg.

During the process of selecting the right wheels for the project, three types were considered:

1) wheels from a Segway i2 SE;
2) wheels from an electric wheelchair;
3) 20-inch wheels from Skyway from BMX.

The analysis of the types of wheels presented above was made based on the most important parameters for the project, i.e., price, availability, and method of assembly. The first option was rejected because of the greater difficulties and costs it would entail. Skyway tires, on the other hand, were considered an inferior option, due to the smaller contact area with the ground and the difficult method of installation.

Ultimately, it was decided to use a wheel from an electric wheelchair, but it was necessary to design an element that would allow it to be combined with a selected motor (Fig. 6). Due to the transmission built into the engine, the combination of elements did not require the use of a complicated design. This feature can be considered an advantage due to the low use of material and quick and easy execution. Four holes drilled in the middle are used to mount the hub to the motor, while the outer holes allow you to attach the wheel (Fig. 7).

Fig. 6. Render of CAD model wheels

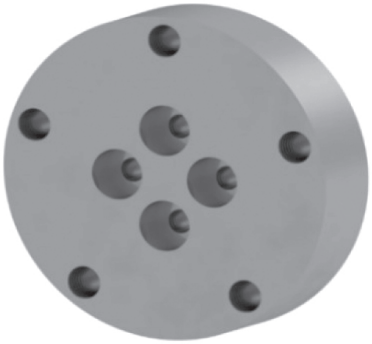

Fig. 7. Render of CAD model of the hub

4.3. Platform steering

In the design process, the most difficult was the design of the steering system (Fig. 8). Since forward and backward movement is achieved by tilting the entire platform in the desired direction, the only purpose of the steering rod is to allow the vehicle to turn. As a result, the proposed solution had to serve this purpose in a clear and intuitive way.

Fig. 8. CAD steering model

Over the past several years, the issue of turning with self-balancing vehicles has been approached in many different ways, but each of them has its drawbacks. Among those worth mentioning are:

- Fixed control stick, at the sides of which two buttons were mounted, each of which was responsible for turning in the right direction [8]. The main disadvantage of this solution is that the driver can only give the command to turn in the selected direction, but he cannot decide on the value of the steering angle.
- Self-centering swivel handle, the turning of which towards the user or in the opposite direction allowed the device to be turned [9]. It was considered that this solution is not very intuitive for the vehicle user.
- Rod mounted on a rotary potentiometer with return springs [10]. In order to make a turn, the entire control stick must be tilted by the desired steering angle in the selected direction.

Due to the fact that the rod rotates on the shaft of the potentiometer, the value of its resistance is proportional to the tilt of the steering system. As a result, the value of the signal delivered to the controller input changes. Despite the fact that this solution allows for precise and smooth control over the steering angle

of the vehicle, it is not ideal due to the low strength of the potentiometer shaft on which the entire structure rests. As described by the creator of this solution, during one of the tests the device was damaged as a result of using too much force.

Due to the occurrence of defects in the above solutions, it was decided to use its own steering rod solution. The design was inspired by the above-mentioned detection of the rod twist using a rotary potentiometer. However, unlike this design, the rotation is performed on a linear shaft with a diameter of 8 mm. This made it possible to use bearings to eliminate resistance on the shaft. The shaft is connected to the clutch, which allows the rotation to be transmitted to the incremental encoder. This solution allows for accurate reading of the deviation set by the user while reducing the risk of damage to the element. The return to the starting position occurs thanks to the springs mounted in one plane with the rod.

4.4. FEM analysis

Due to the bearing arrangement of the control rod, the stresses occurring in it will be small. With this in mind, only the elements of the device body were subjected to static stress analysis using the Finite Element Method. The analysis itself was carried out according to the Hubert criterion.

The following are defined as simulation parameters:

- TETRA type elements with a diameter of 0.1 mm and a gradation coefficient of 1.5. In the end, this allowed to obtain the number of grid elements 946 799, while the number of nodes was 1 600 326.
- The loads were assumed as two forces of 500 N directed perpendicular to the top cover of the platform that act on it. In addition, the force of gravity on the structure was simulated.
- The boundary conditions were set as a fixed bond at the place of mounting the drive unit to the main frame of the structure (visible on the presentation of the analysis results).
- Aluminum 6061 was primarily used as a material. On the other hand, the elements of screw connections were prepared using stainless steel A4 giving the screw class 88. Another material used was PCB plastic, to represent the body of the battery, and the rubber used to cover the tire.

As an effect of carrying out the analysis, the results were obtained from which three parameters were selected as the most important in terms of checking the strength of the structure.

For stresses calculated according to the Huber–Mises stress hypothesis, small values not exceeding 10 MPa were obtained in the place where the sheet metal and the motor housing are in direct contact (Fig. 9).

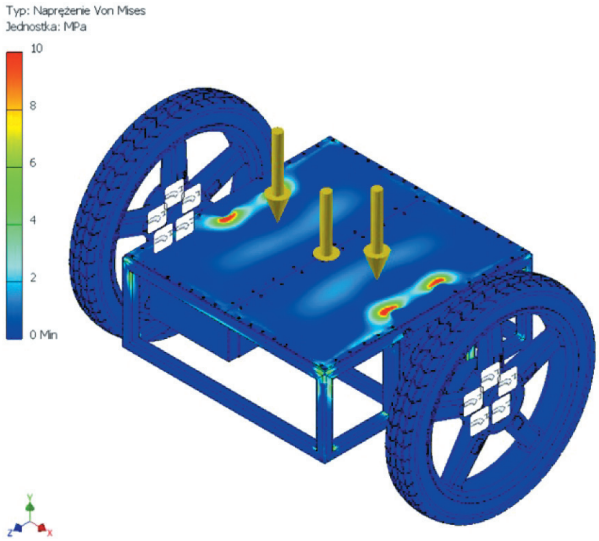

Fig. 9. FEM analysis of the CAD model – stresses

Other results worth to focus on are static displacements and deflections (Figs. 10 and 11). The largest displacement values occur in the center of the platform connection and are equal to approximately 0.16 mm. This value is so small that this change would not be noticed by the user when using the platform.

The last result of the research is the analysis of the safety factor of the structure, which allowed us to assess the strength of the platform.

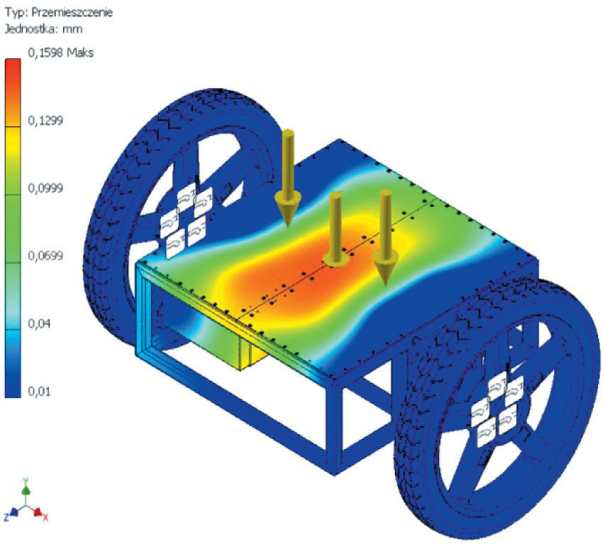

Fig. 10. FEM analysis of the CAD – displacement model

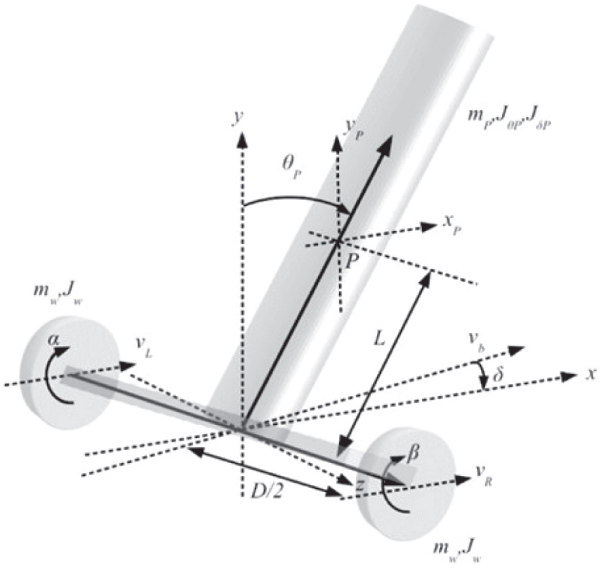

Fig. 11. Simplified human model on a self-balancing vehicle [14]

The safety factor n of a given structural element is determined according to the following formula:

$$k = K / n \Rightarrow n = K / k \tag{7}$$

where:

K – critical stresses,

k – actual stresses on the element.

This should be understood as the ratio of critical stress values to the actual stress values occurring in this element. Therefore, in order for a given structural element not to be plastically deformed under the influence of a given load, the value of this coefficient must be greater than unity [11].

The lowest visible value of the coefficient is 2.63. It follows that no element of the platform will undergo plastic deformation during use.

Summing up the above analysis, it can be concluded that the created structure is able to withstand the load associated with its own weight and that of the passenger on it.

5. INVERTED MATHEMATICAL PENDULUM MODEL

In order to design the control algorithm for the platform, the first step was to consider the model of the inverted mathematical pendulum. This is a common practice when designing self-balancing devices, as a result of which many pins of the discussed model are available, including those Present in the project *Control and balancing of a small vehicle with two wheels for autonomous driving* [12] or in the article *Simulation and control of a two-wheeled self-balancing robot* [13]. In this chapter, the author uses the nonlinear model presented in the article *Mathematical Modelling of Hover Board* [14], which was then linearized and divided into two simpler to control subsystems.

The following assumptions were adopted:

– The friction that occurs in the system is linear friction, which is proportional to the engine speed.
– Friction arising during the reaction of elements with air, due to the significant difficulty of calculations, was not taken into account.
– The efficiency of the gearshift is 1.
– The driver's model was simplified to a rigid body (cylinder) with a height of "2L".
– The starting point of the system relative to the vertical was taken as the top of the base of the structure.

Table 1

Markings – Inverted pendulum

Symbol	Description	Unit
m_k	driver weight	[kg]
m_w	wheel weight (identical for both wheels)	[kg]
$J_{\theta P}$	driver inertia in relation to inclination	[kg·m^2]
$J_{\delta P}$	driver inertia, in relation to roll	[kg·m^2]
J_w	wheel inertia	[kg·m^2]
α_m, β_m	rotation angle (left, right) of the wheel (with respect to the platform)	[rad]
α, β	rotation angle (left, right) of the wheel (relative to the ground)	[rad]
L	distance between base and center of mass of the driver	[m]
θ_p	driver yaw angle (relativeto the ground, where 0 is the vertical position)	[rad]
v_L, v_R	speed of the center (left, right) wheel	[m/s]
x_b, v_b	horizontal coordinate and platform center acceleration (origin)	[m, m/s]
X_p, y_p, z_p	coordinates of the driver's mass center	[m]
D	wheel distance from each other (track width)	[m]
r	circle radius	[m]
ψ	coefficient of viscous friction	[–]
M_L, M_R	torque given to the wheels, by the engine (after transmission)	[Nm]
τ_L, τ_R	torque on the (left, right) engine	[Nm]
ρ	reduction ratio between engine speed and wheel rotation	[–]

For the model presented above, the relationship between the engine, wheels, platform, and driver was determined, which allowed results to be obtained.

Next, a dynamic model was determined, on the basis of which the Lagrange equations of the second kind were written.

The resulting model was non-linear, but it can be linearized to simplify the controller's operation. In order to obtain a stable position of the user on the platform, the target deflection angle of the structure was set at approximately 0 ($\theta_p \approx 0$) and low horizontal rotations were assumed ($\delta \approx 0$).

Thanks to this, the final representation in the state space

$$\dot{x} = Ax + Bu$$

$$x = \begin{bmatrix} \dot{q} \\ \ddot{q} \end{bmatrix} = \begin{Bmatrix} \alpha \\ \beta \\ \theta_p \\ \dot{\alpha} \\ \dot{\beta} \\ \dot{\theta}_p \end{Bmatrix}, \; u = \begin{bmatrix} \frac{1}{\rho} & 0 \\ 0 & \frac{1}{\rho} \\ -\frac{1}{\rho} & -\frac{1}{\rho} \end{bmatrix} = \begin{Bmatrix} \tau_L \\ \tau_R \end{Bmatrix}$$

$$M\ddot{q} + C\dot{q} + Kq = u \Rightarrow \ddot{q} = M^{-1}\left(-Kq - C\dot{q} + u\right)$$

$$x = \begin{bmatrix} \dot{q} \\ \ddot{q} \end{bmatrix} = \begin{bmatrix} \dot{q} \\ M^{-1}\left(-Kq - C\dot{q} + u\right) \end{bmatrix}$$

$$\dot{x} = Ax + Bu = \begin{bmatrix} 0_3 & I_3 \\ -M^{-1}K & -M^{-1}C \end{bmatrix} x + \begin{bmatrix} 0_3 \\ M^{-1} \end{bmatrix} u$$

$$M = \begin{bmatrix} m_1 & m_2 & m_3 \\ m_2 & m_1 & m_3 \\ m_3 & m_3 & m_4 \end{bmatrix}, \; C = \begin{bmatrix} c & 0 & -c \\ 0 & c & -c \\ -c & -c & 2c \end{bmatrix}$$

$$K = \begin{bmatrix} 0 & 0 & 0 \\ 0 & 0 & 0 \\ 0 & 0 & k \end{bmatrix} \tag{8}$$

where:

$$m_1 = \left[\frac{m_p r^2}{4} + \frac{r^2 J_{\delta P}}{D^2} + m_w r^2 + J_w + \frac{J_m}{\rho^2} \right]$$

$$m_2 = \left[\frac{m_p r^2}{4} - \frac{r^2 J_{\delta P}}{D^2} + m_w r^2 + J_w \right]$$

$$m_3 = \left[m_p L r / 2 - J_m / \rho^2 \right]$$

$$m_4 = \left[m_p L^2 + 2J_m / \rho^2 + J_{\theta_p} \right]$$

$$c = \psi / \rho^2, \; k = -m_p g L \tag{9}$$

The above system has a coupling between the steering rod and the platform itself. Thanks to the method presented in the work of Dino Spiller [15], it is possible to divide the discussed case into two separate systems.

The first stage is the transition from the angles of α and β to the parameters of the position of the platform x_b and the angle of deviation δ using the relationship between the wheels and the platform:

$$q_o = \begin{Bmatrix} x_b \\ \delta \\ \theta_p \end{Bmatrix} = \begin{bmatrix} r/2 & r/2 & 0 \\ r/D & -r/D & 0 \\ 0 & 0 & 1 \end{bmatrix} \begin{Bmatrix} \alpha \\ \beta \\ \theta_p \end{Bmatrix} = [S]q \tag{10}$$

The second stage is the introduction of new moments: balancing and rotary. They result from the fact that the joint movement of two motors affects the rectilinear displacement of the platform, while the opposite is responsible for its rotation, which can be written as:

$$q_o = \begin{Bmatrix} \tau_\theta \\ \tau_\delta \end{Bmatrix} = \begin{bmatrix} 1 & 1 \\ 1 & -1 \end{bmatrix} \begin{Bmatrix} \tau_L \\ \tau_R \end{Bmatrix} = [D] \begin{Bmatrix} \tau_L \\ \tau_R \end{Bmatrix}$$

$$\begin{Bmatrix} \tau_L \\ \tau_R \end{Bmatrix} = [D]^{-1} \begin{Bmatrix} \tau_\theta \\ \tau_\delta \end{Bmatrix} = \begin{bmatrix} 0.5 & 0.5 \\ 0.5 & -0.5 \end{bmatrix} \begin{Bmatrix} \tau_\theta \\ \tau_\delta \end{Bmatrix} \tag{11}$$

Thanks to this solution, after substituting into the system from equation (8), we get the desired division into two systems. Moreover, to make it easier to separate the state space system, the order of the state variables has been changed.

$$\dot{x}_N = A_N x_N + B_N u_N =$$

$$\begin{Bmatrix} \dot{x}_b \\ \dot{\theta}_p \\ \ddot{x}_b \\ \ddot{\theta}_b \\ \dot{\delta} \\ \ddot{\delta} \end{Bmatrix} = \begin{bmatrix} 0 & 0 & 1 & 0 & 0 & 0 \\ 0 & 0 & 0 & 1 & 0 & 0 \\ 0 & an_{32} & an_{33} & an_{34} & 0 & 0 \\ 0 & an_{42} & an_{43} & an_{44} & 0 & 0 \\ 0 & 0 & 0 & 0 & 0 & 1 \\ 0 & 0 & 0 & 0 & 0 & an_{66} \end{bmatrix} \begin{Bmatrix} x_b \\ \theta_p \\ \dot{x}_b \\ \dot{\theta}_b \\ \delta \\ \dot{\delta} \end{Bmatrix} + \begin{bmatrix} 0 & 0 \\ 0 & 0 \\ bn_{31} & 0 \\ bn_{41} & 0 \\ 0 & 0 \\ 0 & bn_{62} \end{bmatrix} \begin{Bmatrix} \tau_\theta \\ \tau_\delta \end{Bmatrix} \tag{12}$$

Eventually, two platform subsystems were obtained:

1) base subsystem:

$$\dot{x}_\theta = A_\theta x_\theta + B_\theta \tau_\theta =$$

$$\begin{Bmatrix} \dot{x}_b \\ \dot{\theta}_p \\ \ddot{x}_b \\ \ddot{\theta}_b \end{Bmatrix} = \begin{bmatrix} 0 & 0 & 1 & 0 \\ 0 & 0 & 0 & 1 \\ 0 & an_{32} & an_{33} & an_{34} \\ 0 & an_{42} & an_{43} & an_{44} \end{bmatrix} \begin{Bmatrix} x_b \\ \theta_b \\ \dot{x}_b \\ \dot{\theta}_b \end{Bmatrix} + \begin{bmatrix} 0 \\ 0 \\ bn_{31} \\ bn_{41} \end{bmatrix} \tau_\theta,$$

2) control rod subsystem:

$$\dot{x}_\delta = A_\delta x_\delta + B_\delta \tau_\delta$$

$$\begin{Bmatrix} \dot{\delta} \\ \ddot{\delta} \end{Bmatrix} = \begin{bmatrix} 0 & 1 \\ 0 & an_{66} \end{bmatrix} \begin{Bmatrix} \delta \\ \dot{\delta} \end{Bmatrix} + \begin{bmatrix} 0 \\ bn_{62} \end{bmatrix} \tau_\delta \tag{13}$$

6. STABILIZATION ALGORITHM

6.1. Platform deviation detection

For the proper operation of the stabilization algorithm, it is necessary to read the platform deflection angle from the equilibrium point as quickly and accurately as possible.

To determine it, elements that do not directly indicate the value sought are most often used and are susceptible to various disturbances.

The first of them, i.e. the accelerometer, reads the value of gravitational acceleration. The indicated value changes from the default 9.81 m/s^2 in the case of deviation according to the following formula:

$$V_a = \sin(\theta) + r_a \tag{14}$$

where:

V_a – voltage from accelerometer [V],
θ – angle of deviation [°],
r_a – measurement noise [V].

As can be seen, this equation is not linear, however, for the value of θ ca. 20°, one can assume the linear relation $\sin(\theta) = \theta$ according to [16], resulting in which we get:

$$\theta \approx V_a - r_a \tag{15}$$

The disturbances r_a included in the above formula are the result of other accelerations (longitudinal and lateral) and vibrations that arise when the vehicle is moving. Therefore, the data received from the accelerometer contains a significant amount of noise, so that when designing self-balancing devices, you cannot rely only on their readings.

The second type of sensor from which one can get the necessary data is the gyroscope. This device allows the measurement of the rate of change of the angle ω, which by integrating after time allows you to determine the desired value of the angle of deviation. Thanks to this, the parasitic accelerations acting in the system do not affect the result obtained as much as in the case of the accelerometer [16].

Unfortunately, one cannot rely on gyro readings due to zero errors (so-called bias). As a consequence, with the increasing duration of operation, there is an increase in the so-called drift, i.e. the error of the tilt angle [16].

As presented in the paragraphs above, both sensors are better suited for certain types of measurements. For long measurement periods, the accelerometer works better due to the lack of drift, but with short measurements a gyroscope will obtain more accurate results due to the reduced susceptibility to interference. As can be seen, the sensors complement each other's imperfections, therefore it is a common practice to merge data obtained from the above-mentioned devices.

6.2. Fusion of measurement signals

One of two filters can be used to synthesize signals from sensors: a complementary one, which is a simpler but worse method, and a Kalman filter that allows more accurate results to be obtained, but with a higher demand for computing power.

The operation of the complementary filter is based on complementing each other's data from sensors, none of which fully reflects the actual result. Determining the tilt angle on the basis of the two sensors in question involves the use of appropriate filters: low-pass for the accelerometer to remove fast-shift errors, high-pass is used for the gyroscope to remove slow-changing errors (drift) to then sum up the obtained values as shown in the following equation [17]:

$$\theta_f = K_1 \left(\theta_{f-1} + \dot{\theta}_g \cdot T_s \right) + K_2 \cdot \theta_a \tag{16}$$

where:

θ_f – angle estimated value [°],
θ_{f-1} – angle estimated value [°],
θ_a – angle value based on accelerometer [°],
$\dot{\theta}_g$ – angle estimated value [°],
K_1, K_2 – complementary filter factor (for gyroscope and accelerometer respectively).

As can be seen, this filter is easy to implement, because it can be implemented with a single line of code, which saves resources of the computing unit. However, the problem in the case of its use is the determination of appropriate values of coefficients, which have a decisive impact on the accuracy of the results obtained.

The Kalman filter is a commonly used algorithm that allows the determination of the value of a variable that is not available using measurable values and a mathematical model that determines the relationships between both quantities. In the case of linear systems, we use its basic version, while for nonlinear models it is necessary to use an extended Kalman filter. In the previous section, it was shown that with small deviations, the determination of the angle can be treated as a linear model.

In order to analyse the principle of filter operation, it is necessary to consider the mathematical model of the discrete system on which the noise acts.

$$x_k = A \cdot x_{k-1} + B \cdot u_{k-1} + w_{k-1}$$
$$z_k = H \cdot x_k + v_k \tag{17}$$

where:

A – transition matrix,
B – input matrix,
w_{k-1} – system (process) noise,
H – matrix of state association with measurement,
v_k – measurement noise.

Both of these noises are assumed to be like white Gaussian noises, independent of each other with a distribution:

$$p(w) \sim N(0,Q),\ p(v) \sim N(0,R) \tag{18}$$

where Q, R – matrix of covariance of the process and measurements respectively.

The operation of this algorithm consists in the cyclical estimation of the searched state vector along with its covariance.

This process can be divided into two stages:

1) Prediction phase, in which values are predicted (a priori) based on data from the previous step:
   – state vector:

$$\hat{x}_k^- = A \cdot \hat{x}_{k-1} + B \cdot u_{k-1} \tag{19}$$

   – covariance matrix of filtration errors:

$$P_k^- = A \cdot P_{k-1} \cdot A^T + Q \tag{20}$$

2) Correction phase, in which the data received from the previous part is corrected (updated), thanks to the information received from the sensors [17].

At this stage, we specify:

– determination of Kalman filter gain:

$$P_k^- = A \cdot P_{k-1} \cdot A^T + Q \tag{21}$$

where S_k – innovation of covariance is calculated as

$$S_k = \left(H \cdot P_k^- \cdot H^T + R\right)^{-1} \tag{22}$$

– updating the state vector $\hat{x}$ using the measurement vector y_k, the so-called innovation referred to as:

$$y_k = \left(z_k - H \cdot \hat{x}_k^-\right) \tag{23}$$

where z_k – measurement from the sensor

$$\hat{x} = \hat{x}_k^- + K_k \cdot y_k \tag{24}$$

– the last step is to update the covariance matrix for the next algorithm loop:

$$P_k = (I - K_k \cdot H) P_k^- \tag{25}$$

where I – unit matrix.

As can be seen from equation (25), the Kalman gain allows one to determine how much the results of measurements from the correction phase will affect the estimated state. In the case of small gain, we rely more on prediction than on measurements (we consider sensor data uncertain), while with large K values, the data measured at the time of determination plays a more important role.

In order to check the operation of both filters, a simulation of the operation of reading tilt angle data along with the interference present on both types of sensors was prepared. The obtained results are presented in Figure 12.

As can be seen, the impact of interference present on the sensors is definitely more noticeable in the case of a complementary filter. The Kalman filter, on the other hand, estimates the actual value of the deflection angle very well.

It follows that in the case of the discussed project it was required to use the Kalman filter, due to the importance of precise determination of the platform deflection angle with a self-balancing algorithm.

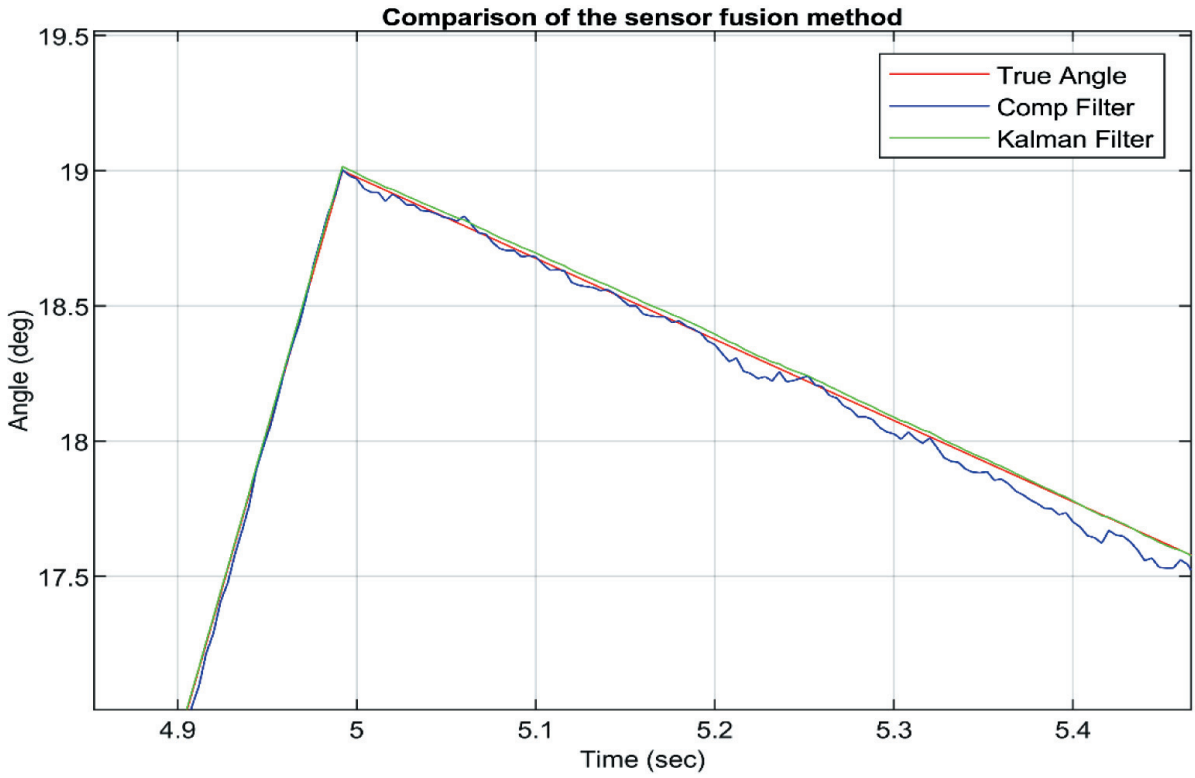

Fig. 12. Chart comparing the operation of selected filters when determining the angle of deviation of the platform

6.3. LQR controller

While working on the stabilizing algorithm, the selection of various control methods was considered, however, due to the important aspect of energy control signal cost in mobile projects, it was decided to choose the LQR controller, whose task is to minimize the square quality index J determined by the following formula:

$$J = \int_0^{\infty} \left(x^T Q x + u^T R u \right) dt \tag{26}$$

where:

Q – input (control signal) weight array,
R – matrix of state weights.

Minimizing the above-mentioned indicator allows one to obtain the value of the K gain vector, which is used in the control law:

$$u = -Kx \tag{27}$$

The vector K is described by the formula:

$$K = R^{-1} B^T P \tag{28}$$

In order to determine the P matrix in the above equation, it is necessary to solve the Riccati equation:

$$A^T P + PA + Q - PBR^{-1} B^T P = 0 \tag{29}$$

However, in order to use this equation to obtain a finite number of solutions, it is necessary that the system for which the LQR regulator is selected is a controllable system [18]. A system can be considered controllable when the rank of the controllability matrix is equal to the order of the system.

The matrices Q and R should be diagonal matrices with non-negative values. The first matrix informs us how important it is for the system to obtain the exact value of the state variable. The second matrix indicates how much energy expenditure can be spent on controlling parameters.

6.4. Stabilizing algorithm – matlab environment

In its first part, models of the state space of the steering rod and base subsystems were created. Then, for each of them, the following scheme of operation was used for control.

As can be observed, the regulator fulfilled the task of moving the poles from the positive part of the graph to the desired negative part.

Then, for each of them, the following scheme of operation was used for control:

- Check the controllability and observability of the system to verify the applicability of the LQR controller.
- After verifying the above-mentioned properties of the system, the parameters of the controller in question were selected. Therefore, the next step is to perform discretization of the system. To do this, the *c2d ()* command was used, with selected "ZOH" as the discretization method (maintaining the state until the next sample).
- Having a discretized system, it was necessary to set the values in the matrices Q and R, which with the command *dlqr ()* allowed to determine the gain vector K.
- In order to implement the LQR controller, a new system was created based on the obtained vector K.
- In order to determine the efficiency of the controller, the positions of the poles of the original subsystem were compared with the poles of the newly obtained system, as illustrated in the graphs below (for comparison, in a continuous version with the same values of Q and R).

As can be observed in Figure 13, the regulator fulfilled the task of moving the poles from the positive part of the graph to the desired negative part.

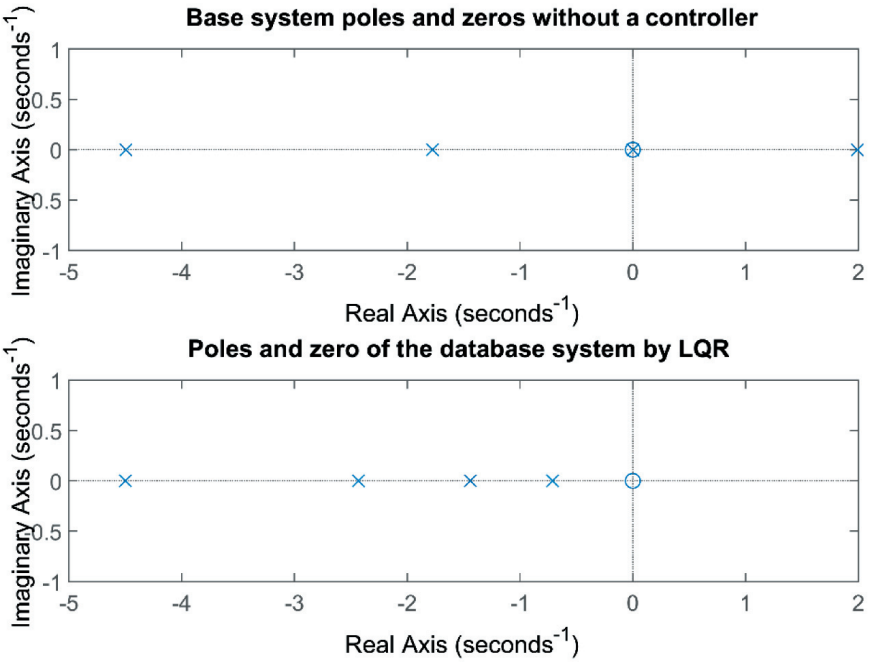

Fig. 13. Pole and zero graph (continuous) system without and with LQR regulator

6.5. Stabilizing algorithm – Simulink simulation

Bearing in mind that the verification of pole positions alone does not give accurate information about the behavior of the system, the simulation of model was carried out in Simulink module (Fig. 14).

This simulation was carried out in the main model, which included a subsystem mapping the behavior of the designed self-balancing structure and LQR regulators of the steering rod and base (Figs. 15–17).

The operation of the system was checked using a reference signal in which the linear velocity and angular velocity of the steering rod were set (the position of the platform and the angle were obtained as a time derivative of velocity integration).

The tilt angle of the platform was not used, which might seem the most intuitive in connection with its actual control, but it would cause a violation of the equilibrium condition of the inverted pendulum in the simulation, which is the base subsystem. As a result, the correct results would not be obtained.

In the subsystem mapping the behavior of the designed self-balancing structure, a block containing a nonlinear model derived from the analysis of the inverted pendulum problem was created. On its basis, the reading of the tilt angle of the platform using an accelerometer and gyroscope was simulated.

Thanks to this, it was possible to verify the sensory fusion discussed earlier.

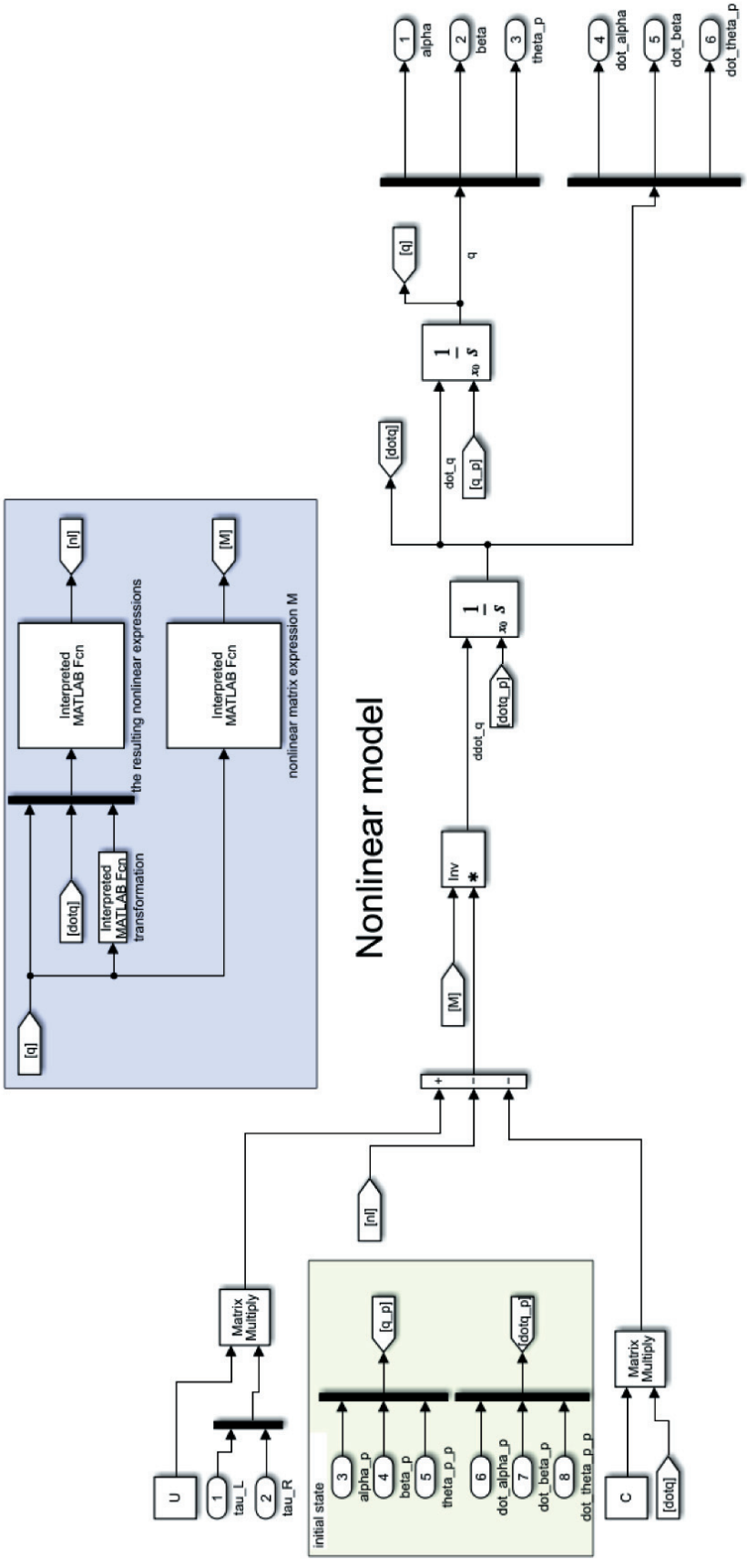

Fig. 14. Nonlinear platform model

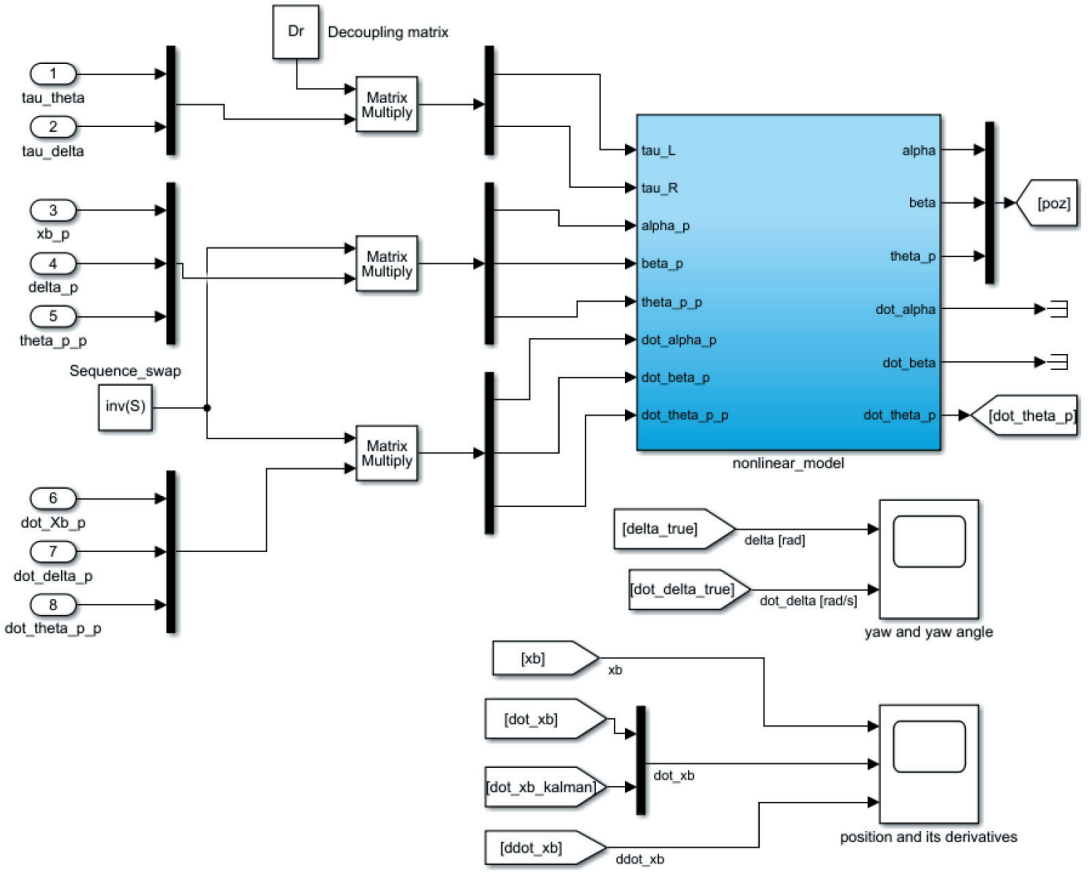

Fig. 15. Simulink model of the controlled object (part 1 of 2)

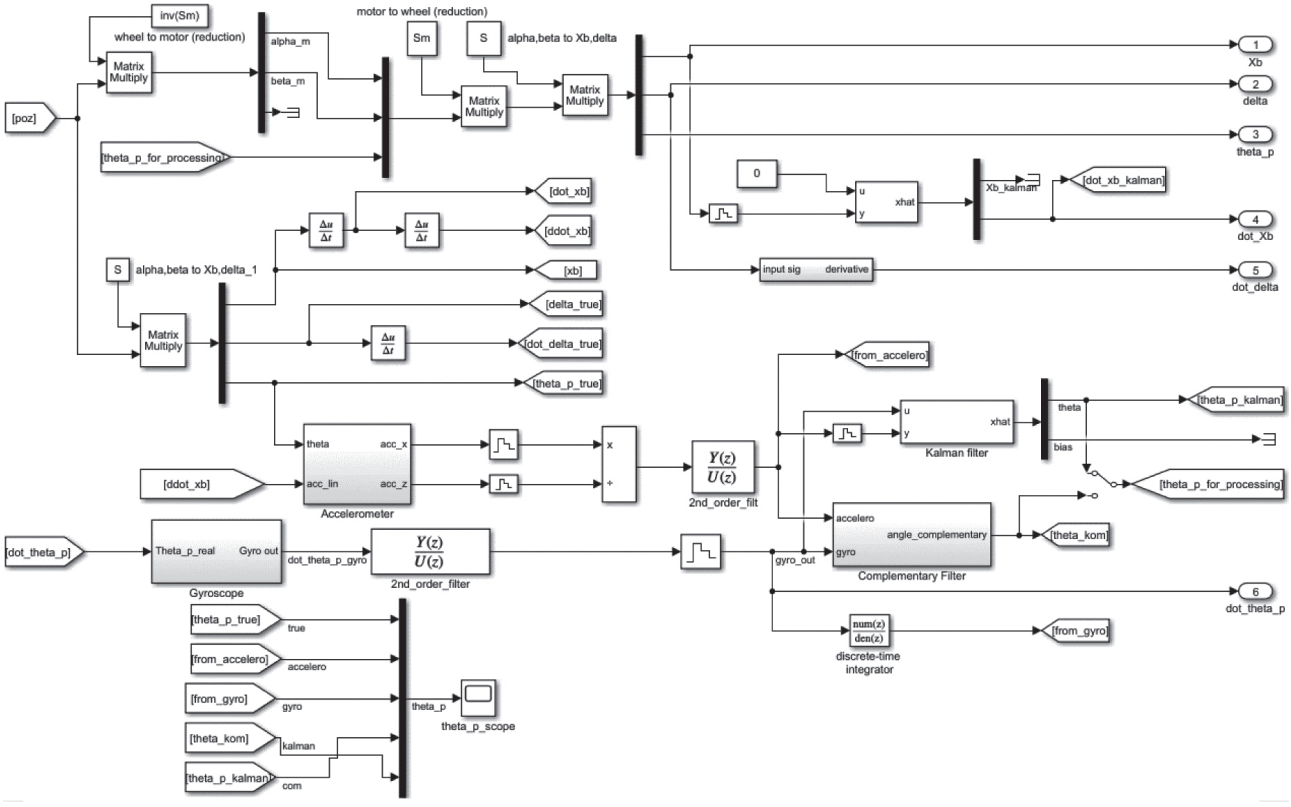

Fig. 16. Simulink model of the controlled object (part 2 of 2)

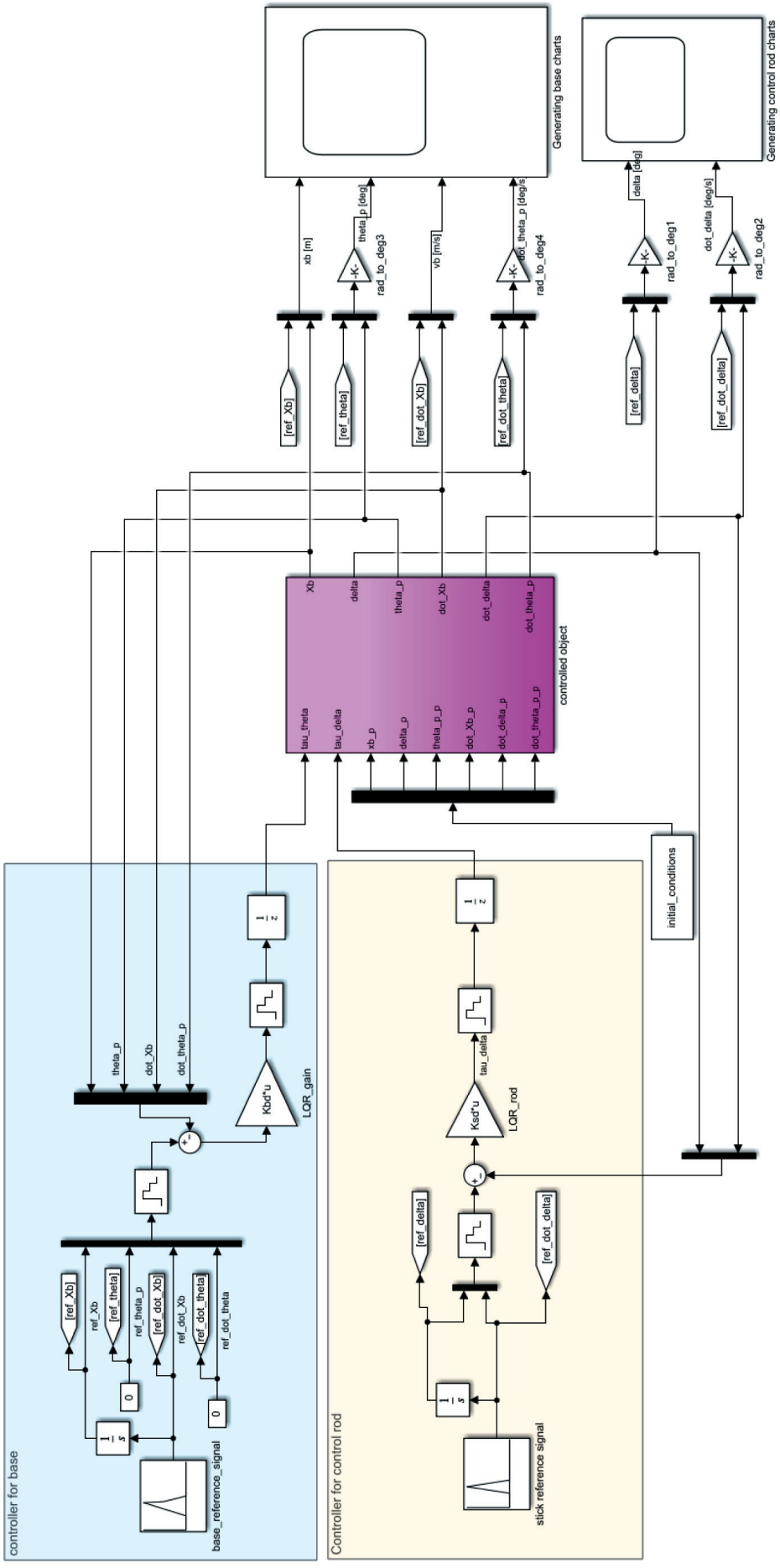

Fig. 17. Main simulink model of the stabilization algorithm

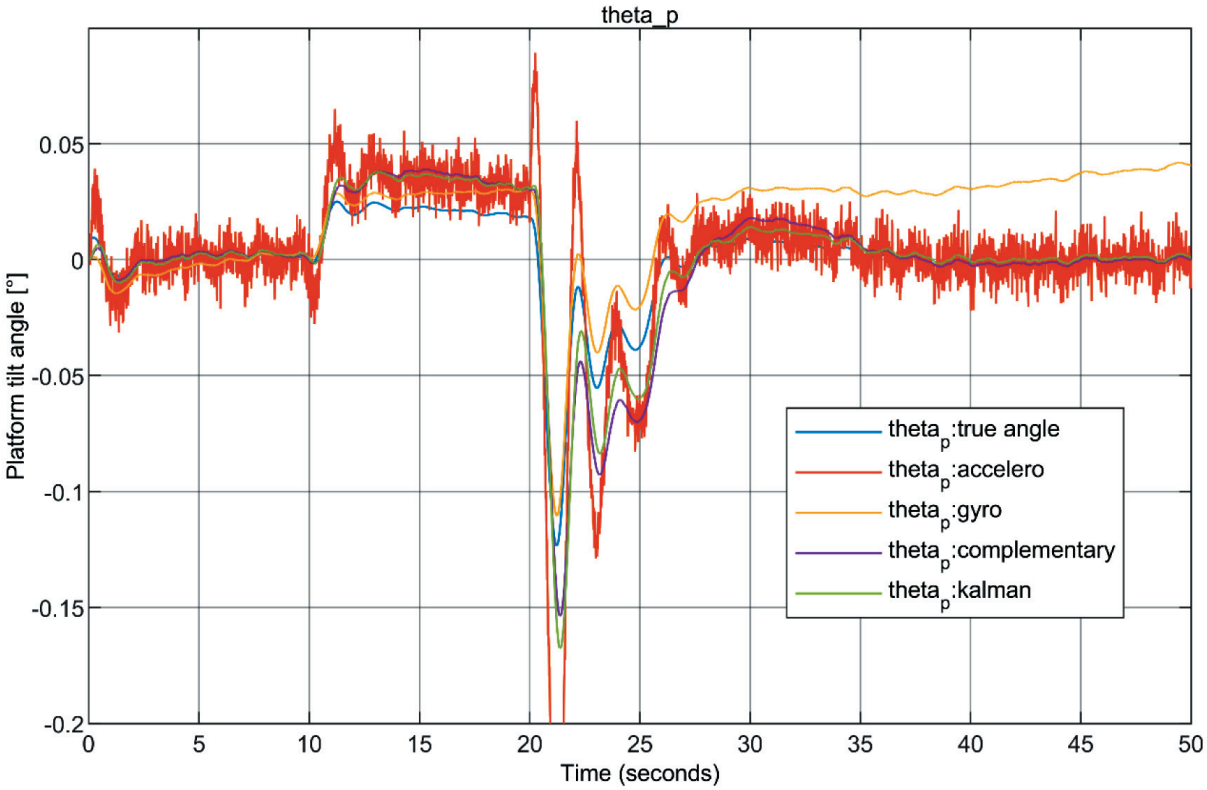

Fig. 18. Chart comparing methods for reading the angle of deviation of the platform

The graph presented in Figure 18 allowed us to show the difference between the data derived from the sensors and the data obtained with the help of the filters used.

As one can see, the data obtained from the model allows us to draw the same conclusions as in the subsection on sensory fusion. The influence of changes in platform velocity on the accuracy of the deviation indication obtained from the accelerometer is clearly visible. Another case that has been confirmed is the increasing drift of the gyroscope over time. The last result that has been re-verified is the greater accuracy of the Kalman filter over the complementary filter.

As mentioned at the beginning of the subsection, the created model was subjected to the influence of a reference signal in order to try to select appropriate values for the Q and R matrix for both regulators.

Table 2

LQR regulator settings for individual subsystems

Matrix	Base layout	Stick layout
Q	diag (20,70,4,0.2)	diag (4,5)
R	0.1	0.005

For each subsystem, the following results were obtained:

1) Base subsystem.

   Under the influence of the speed task, the tilt of the platform underwent changes adequate to the changes in the state of the system (Fig. 19). Despite many attempts, it was not possible to choose the ideal parameters for the Q and R matrix of the base system. In this case, there are two potential options to consider: further attempts to obtain fully satisfactory results using the parameter space search method, or the use of e.g., machine learning to determine the settings, as presented in the "Mendel" journal article [19].

2) Steering rod subsystem.

   In Figure 20 it can be seen that the coefficients in the matrices have been selected correctly. The simulation model reacts with the required speed and accuracy to the set parameters. Due to the fact that the steering rod system is the SISO type, the desired results have been achieved.

In conclusion, the created stabilizing algorithm works as intended. Nevertheless, in order to achieve a fully satisfactory result, further work on the selection of coefficients is required.

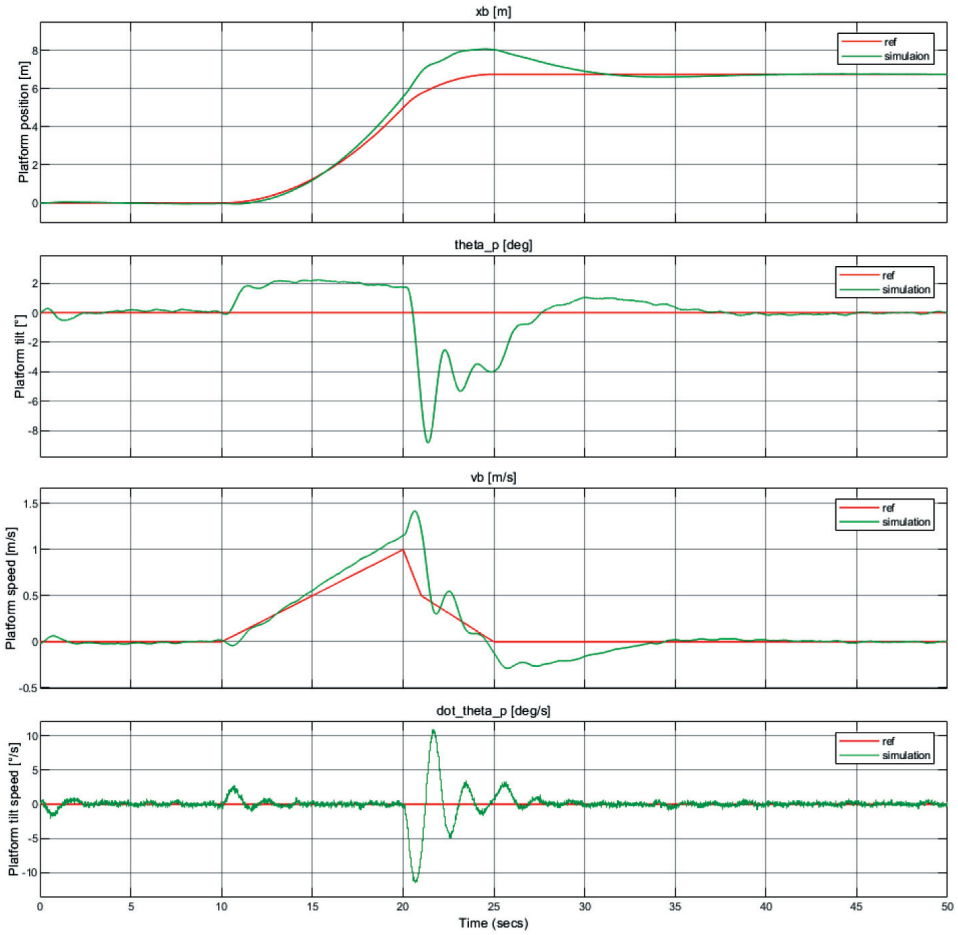

Fig. 19. Place comparison of the reference signal with the system response in the case of the construction base

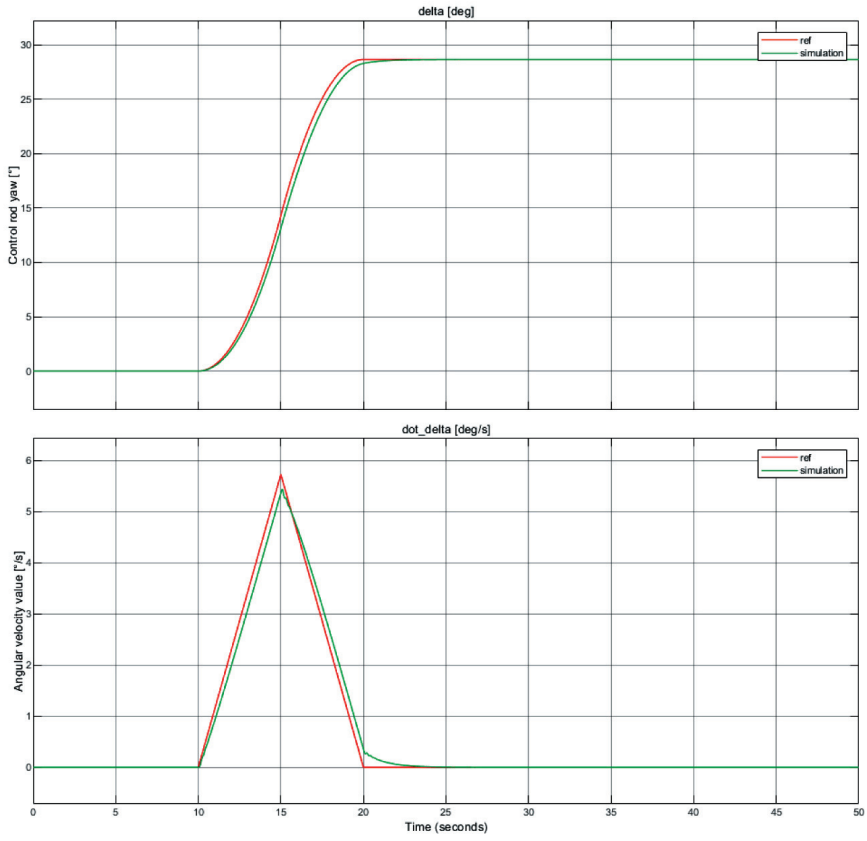

Fig. 20. Comparison of the reference signal with the system response in the case of the control rod

7. SUMMARY

All of the stages related to the design of the structure have been completed. Further work related to the development of the project should be directed in order to create an actual structure. This is due to the fact that even the best prepared mathematical model or designed structure can behave differently in the case of physical implementation. In addition, operating on a real model would allow the acceleration of the selection of the parameter settings of the controllers of individual systems. Another direction of development may be to design shields for the platform, which would reduce the risk of damage to elements.

To sum up, the model presented in the work is considered completed in terms of the theoretical aspects, however its further development requires experiments with a real prototype. Due to the high building costs associated with this model, this task exceeded the scope of this paper.

Reference

[1] Janczewska D.: *Zrównoważony rozwój z perspektywy mikromobilności*. Zarządzanie Innowacyjne w Gospodarce i Biznesie 2020, 29, 2: 165–187.

[2] *Ustawa z dnia 30 marca 2021 r. o zmianie ustawy – Prawo o ruchu drogowym oraz niektórych innych ustaw*. Dz.U. z 2021 r., poz. 720.

[3] Fryar C.D., Kruszon-Moran D., Gu Q., Ogden C.L., *Mean body weight, weight, waist circumference, and body mass index among adults: United States, 1999–2000 through 2015–2016*. National Center for Health Statistics (U.S.), USA, December 20, 2018.

[4] *Rozporządzenie Ministra Transportu i Gospodarki Morskiej z dnia 2 marca 1999 r. w sprawie warunków technicznych, jakim powinny odpowiadać drogi publiczne i ich usytuowanie*. Dz.U. z 2016 r., poz. 124.

[5] The Robot MarketPlace. http://www.robotcombat.com/products/NPC-T74.html [10.05.2021].

[6] L. Shenzhen Center Power Technology Co., CP12120 [product catalog].

[7] Adamczyk M., Gawrońska K., Szczepanowska-Wołowiec B., Lorkowski J., Kotela A., Hładki W., Kotela I.: *Ocena budowy anatomicznej stóp u studentów Uniwersytetu Jana Kochanowskiego w Kielcach*. Ostry Dyżur 2016, 9, 3: 73–76.

[8] Stoppi. Homemade Physics Experiments: *Segway*. https://stoppi-homemade-physics.de/segway [5.11.2021].

[9] Baker N., Brown C., Dowling D., Modra J., Tootell D., Cazzolato B.: *State-Space Control of Electro-Drive Gravity-Aware Ride Final Report*. 2006.

[10] Johnston I.: *Project 012 – Home Built Segway*. https://www.ianjohnston.com/index.php/projects/48-project-012-home-built-segway [10.11.2021].

[11] Machniewicz T.: *Podstawy wytrzymałości materiałów. IMiR – MiBM – Wykład nr 2. Osiowe rozciąganie i ściskanie.* http://zwmik.imir.agh.edu.pl/dydaktyka/dla_studentow/imir/IMiR_PWM_Wyklad_02%20-%20Rozciaganie%20i%20sciskanie.pdf [15.01.2022].

[12] Batmanian S., Naga P.: *Control and balancing of a small vehicle with two wheels for autonomous driving*. KTH Royal Institute of Technology 2019 [master thesis].

[13] An W., Li Y.: *Simulation and control of a two-wheeled self-balancing robo*t. IEEE International Conference on Robotics and Biomimetics (ROBIO), Shenzhen, China, 2013, pp. 456–461.

[14] Sangotra D.I., Mendhe M., Kshirsagar S.D., Tamboli R.: *Mathematical Modelling of Hover Board*. Journal of Physics: Conference Series, May 2021, 1913, 1.

[15] Spiller D.: *Model-based development of a self-balancing, two-wheel transporter*. University of Padua, Department of Technology and Management of Industrial Installations 2017 [master thesis].

[16] Pasaye J.R., Valencia J.A.B., Pérez F.J.: *Tilt measurement based on an Accelerometer, a Gyro and a Kalman Filter to control a self-balancing vehicle*. 2013. https://ieeexplore-1ieee-1org-100004799007c.wbg2.bg.agh.edu.pl/stamp/stamp.jsp?tp=&arnumber=6702711 [15.11.2021].

[17] Chudzik S.: *Zastosowanie tanich czujników inercyjnych w układzie regulacji kąta pochylenia pojazdu balansującego*. Przegląd Elektrotechniczny 2015, 91, 6: 177–180.

[18] Tryma J.: *JT – Automatyka i programowanie*. Jtjt.pl, http://jtjt.pl/odwrocone-wahadlo [10.11.2021].

[19] Marada T., Matousek R., Zuth D.: *Design of Linear Quadratic Regulator (LQR) Based on Genetic Algorithm for Inverted Pendulum*. Mendel 2017, 23, 1: 149–156.

SZYMON RĘCZKOWICZ, Eng.
AGH University of Science and Technology
al. A. Mickiewicza 30, 30-059 Krakow, Poland
szymon.reczkowicz@gmail.com